AMS Home   Journals Home   Journal Archive   Subscribe   For Authors   Help   Advanced Search   Search   Go

Full Text View

A Dissipation Integral with Application to Ocean Diffusivities and Structure

Edwin K. Schneider and Uma S. Bhatt

Center for Ocean–Land–Atmosphere Studies, Calverton, Maryland

ABSTRACT

An integral balance is developed for steady fluid flows relating dissipation in volumes bounded by isosurfaces of a tracer (quasi-conserved quantity) and solid boundaries to the covariance of the tracer value and surface fluxes across the boundaries. The balance is used to estimate upper bounds for vertical eddy diffusion coefficients for temperature and salinity in various volumes of the ocean. The vertical temperature diffusivity is calculated to be small, $O(0.1 \times 10^{-4} \text{ m}^2 \text{ s}^{-1})$, except for the warmest and coldest volumes of the ocean. The vertical salinity diffusivity for the volume that makes up most of the deep ocean is estimated to be $O(1 \times 10^{-4} \text{ m}^2 \text{ s}^{-1})$. Sources of error in these calculations are discussed, and the sensitivity to errors in the surface flux data is evaluated.

The dissipation integral is also applied to demonstrate some related results concerning extrema and homogenization. The Prandtl–Batchelor theorem is a special case of one of these results. As a consequence of these results, if turbulent transfer is downgradient and there are no internal sources or sinks, a necessary (but not sufficient) condition for a climatological tracer distribution to be in a steady state is the absence of internal extrema. The climatological salinity distribution does not appear to violate this condition.

Options:
- Create Reference
- Email this Article
- Add to MyArchive
- Search AMS Glossary

Search CrossRef for:
- Articles Citing This Article

Search Google Scholar for:
- Edwin K. Schneider
- Uma S. Bhatt

1. Introduction

Advection can be eliminated from volume integrals of fluid conservation laws in certain special cases, leading to increased understanding of the structure of fluid flows. Schneider (1977) used this approach in a two-dimensional case to make some deductions about the distribution of angular momentum in the atmosphere. It was shown there that the advection terms of the equation for conservation of angular momentum in a steady, axially symmetric atmospheric flow, integrated over a region bounded by a surface of constant angular momentum, is zero. This result was then used to show that, if the fluxes of

angular momentum by transient and small-scale motions are downgradient, then there can be no maxima or minima of angular momentum in the interior of a steady zonally averaged atmosphere. Maxima and minima can form only adjacent to solid boundaries. This result generalized the result of Hide (1969) that westerlies could not form at the equator under similar restrictions.

Another example of a useful result that can be obtained by choosing a region in which the volume integrated advective tendency disappears arises in steady two-dimensional flows. Because there is no advection across streamlines, the tendency due to advection integrated over an area bounded by a streamline is zero. As described by Pedlosky (1996), this result is used in two dimensions in the derivation of the Prandtl–Batchelor theorem to infer homogenization of a conserved quantity inside a bounding streamline, in the limit of vanishing downgradient diffusion (Batchelor 1956).

Walin (1982) showed how the vanishing of the advective fluxes of temperature across volumes bounded by surfaces of constant temperature and solid boundaries could be used to infer an effective vertical diffusivity at these surfaces. Niiler and Stevenson (1982) used similar arguments to infer properties of the ocean circulation from the surface heat flux. These studies extended inferences from the vanishing of volume integrated advective fluxes to three dimensions. Zhang and Talley (1998) have used the same technique to estimate diapycnal and diathermal diffusivities for various regions of the World Ocean. Speer (1997) applied a version of Walin's technique (also described by Garrett et al. 1995), which allows advective fluxes across internal surfaces to be specified, to estimate diapycnal diffusivities for the North Atlantic.

Here the volume integrated approach is extended to higher moments. An integral balance is developed for steady flows that relates the dissipation of a tracer (quasi-conserved quantity), integrated over a volume bounded by isosurfaces of the tracer and solid boundaries, to the covariance of the tracer and the tracer flux integrated over the surface of the volume.

Several applications of the dissipation integral are presented. Estimates of the dissipation rates for temperature and salinity variance are obtained for different layers of the ocean bounded by isothermal and isohaline surfaces, respectively, using surface fluxes and observations of the time mean temperature and salinity. Assuming that the turbulent transfer can be represented by vertical eddy diffusion, the dissipation rates and internal tracer structure of the ocean are used to estimate upper bounds for the diffusion coefficients. Next, a tracer homogenization result resembling the Prandtl–Batchelor theorem is proved when turbulent transfer is assumed to be downgradient for finite amplitude diffusivity and three dimensions. Also, results are developed relating extrema of a tracer to internal sources or boundary fluxes. As an application of these results, the climatological salinity distribution is examined and found to be consistent with the conditions of steady state, downgradient turbulent transfer, and no internal sources or sinks.

2. Derivation of the dissipation integral

An incompressible fluid will be assumed for simplicity, but analogous relationships can be derived in the compressible case.

1) In a steady state, the integrated advection of a conserved quantity T by the time mean motions over a volume bounded by a surface of constant time mean T and solid boundaries is zero. In the absence of internal sources and sinks, the net turbulent flux across the surface of this volume must then also be zero.

This result was derived and used by Schneider (1977) in the two-dimensional case and Niiler and Stevenson (1982) and Walin (1982) in three dimensions. The result follows from the steady-state conservation equation

$$\mathbf{v} \cdot \nabla T = Q = -\nabla \cdot \mathbf{F} + S. \quad (1)$$

Equation (1) represents a turbulent flow where v is the three-dimensional time mean velocity field, T is a time mean scalar quantity, and the balance is steady state in the sense that the time means are not changing for sufficiently long averaging intervals. Additionally, the source term Q is taken to be composed of the convergence of a flux $\mathbf{F}$ of T due, for example, to transients and small-scale mixing plus other internal sources and sinks S. The specified sources and sinks will be considered in section 2d.

The incompressible fluid satisfies the mass continuity equation

$$\nabla \cdot \mathbf{v} = 0, \quad (2)$$

and the normal velocity vanishes at a solid boundary B, so

$$\mathbf{v} \cdot \mathbf{n} = 0 \text{ on } B, \quad (3)$$

where $\mathbf{n}$ is the outward directed unit vector normal to B. Equation (1) is integrated over volume V surrounded by surface

C. The advection term on the lhs of (1) is rewritten as $\mathbf{v} \cdot \nabla T = \nabla \cdot (\mathbf{v}T) - T \nabla \cdot \mathbf{v}$, and the second term on the rhs of this relation is zero from (2). Denoting the volume integral by angle brackets, $\langle \mathbf{v} \cdot \nabla T \rangle = \langle \nabla \cdot (\mathbf{v}T) \rangle$. Applying Gauss's divergence theorem gives $\langle \mathbf{v} \cdot \nabla T \rangle = \iint_C (T\mathbf{v} \cdot \mathbf{n}) \, da$. Then, using Gauss's theorem on the flux divergence term, the volume integral of (1) with $S = 0$ is

$$\iint_C (T\mathbf{v} \cdot \mathbf{n}) \, da = \langle Q \rangle = -\iint_C (\mathbf{F} \cdot \mathbf{n}) \, da. \quad (4)$$

The surface C is composed of solid surfaces B (at which the normal velocity is zero) and permeable (i.e., internal to the fluid) surfaces P so that $C = B + P$. A schematic of this configuration is shown in Fig. 1a ⊙⁻. Integrating (2) over V,

$$\iint_C (\mathbf{v} \cdot \mathbf{n}) \, da = \iint_P (\mathbf{v} \cdot \mathbf{n}) \, da = 0 \quad (5)$$

since the normal velocity is locally zero on B. If the bounding surface C is now taken to be composed of internal surfaces P of constant $T = T_1$ connecting solid boundaries B, then using (3) and (5)

$$\iint_C (T\mathbf{v} \cdot \mathbf{n}) \, da = T_1 \iint_P (\mathbf{v} \cdot \mathbf{n}) \, da + \iint_B (T\mathbf{v} \cdot \mathbf{n}) \, da$$

$$= 0. \quad (6)$$

Therefore, from (4) and (6),

$$\iint_C (\mathbf{F} \cdot \mathbf{n}) \, da = 0. \quad (7)$$

The net advective flux across the boundary is zero because the normal velocities are zero at the solid boundaries B and because the net mass flux across the internal, constant T, boundary P is zero. Consequently, the net turbulent flux across the boundary C is also zero. The steady-state assumption additionally constrains the global integral of Q to be zero.

2) Consider a volume V bounded by a surface P of constant $T = T_1$ and solid surface B. The net flux into V across B is balanced by an equal net flux out of V across P.

It follows directly from (7), by splitting the integral into the contributions from the two subsurfaces, that

$$-\iint_B (\mathbf{F} \cdot \mathbf{n}) \, da = \iint_P (\mathbf{F} \cdot \mathbf{n}) \, da. \quad (8)$$

3) The covariance of $\mathbf{F}$ with the gradient of T averaged over the same V can be determined from the distribution $\mathbf{F}$ and T at the solid boundaries.

Since $T(\mathbf{v} \cdot \nabla T) = \mathbf{v} \cdot \nabla (T^2/2) = \nabla(\mathbf{v}T^2/2)$, multiplying (1) with $S = 0$ by T and integrating over V gives

$$-\langle T\nabla \cdot \mathbf{F} \rangle = 0. (9)$$

Integrating (9) by parts,

$$0 = -\langle T\nabla \cdot \mathbf{F} \rangle = -\langle \nabla \cdot (T\mathbf{F}) \rangle + \langle \mathbf{F} \cdot \nabla T \rangle.$$

Then

$$= \iint_B (T\mathbf{F} \cdot \mathbf{n}) \, da + T_1 \iint_P (\mathbf{F} \cdot \mathbf{n}) \, da.$$

Finally, using (8), the relationship

$$\langle \mathbf{F} \cdot \nabla T \rangle = \iint_B (T - T_1)(\mathbf{F} \cdot \mathbf{n}) \, da \qquad (10)$$

is obtained. Equation (10) is the simplest form of the integral dissipation balance. It is a local generalization of a result found by Stern (1975) for the balance between dissipation (lhs) and production (rhs) of salinity variance over a full ocean basin and is used by Joyce (1980) for the balance between dissipation and production of thermal variance over the World Ocean.

If V is bounded by two surfaces of constant T, T_1 and T_2, and solid boundaries (see schematic in Fig. 1b ⊙⇒), then (10) may be applied to V_1 bounded by T_1 and B_1, as well as to V_2 bounded by T_2 and B_2 and the results subtracted, giving

$$\langle \mathbf{F} \cdot \nabla T \rangle = \iint_{B_2} (T - T_2)(\mathbf{F} \cdot \mathbf{n}) \, da$$

$$- \iint_{B_1} (T - T_1)(\mathbf{F} \cdot \mathbf{n}) \, da. \qquad (11)$$

4) General integral balance for arbitrary functions of T and specified forcing.

The results above can be generalized to an arbitrary twice differentiable function of T, $f(T)$, and also to include specified sources and sinks S. Multiplying (1) by $f'(T)$ and using $\nabla f(T) = f'(T)\nabla T$, the equation

$$\mathbf{v} \cdot \nabla f(T) = -f'(T)\nabla \cdot \mathbf{F} + f'(T)S \qquad (12)$$

is obtained. The integral of the lhs of (12) over volumes bounded by surfaces of constant T and solid boundaries disappears as before. The result analogous to (7) obtained from (1) with nonzero S is

$$\iint_C (\mathbf{F} \cdot \mathbf{n}) \, da = \langle S \rangle, \qquad (13)$$

while the generalization of (10) is

$$\langle f''\mathbf{F} \cdot \nabla T \rangle = \iint_B (f' - f'_{T=T_1})(\mathbf{F} \cdot \mathbf{n}) \, da - \langle f'S \rangle. \qquad (14)$$

To obtain (10) from (14), $f(T) = T^2/2$ and $S = 0$ are used.

3. Application to ocean diffusivities

Estimates of the diffusivity of temperature and salinity using the dissipation method, based on (11), are presented in this section. The methodology is described in section 3a. Estimates of temperature diffusivity using observational datasets and the associated potential errors are discussed in section 3b. Salinity diffusivity estimates made using observations of the salinity distribution and surface fluxes from an atmospheric reanalysis are given in section 3c.

a. Method

The dissipation integral per unit volume between surfaces T_1 and T_2, defined as $D \equiv -\langle \mathbf{F} \cdot \nabla T \rangle / V$, is found from [(11)](#) to be

$$D = \left(\iint_{B_1} (T - T_1)(\mathbf{F} \cdot \mathbf{n}) \, da - \iint_{B_2} (T - T_2)(\mathbf{F} \cdot \mathbf{n}) \, da \right) \bigg/ V. \quad (15)$$

The surface fluxes as well as the surface and interior distributions of T are needed to evaluate D. Evaluation of the quantity DV depends only on surface information.

An approach similar to that of Stern (1977), [Joyce (1980)](#), and [Walin (1982)](#) is used to obtain estimates of "average" diffusion coefficients in the ocean. In order to apply this approach, it is assumed that turbulent fluxes result from vertical diffusion. Here, as in the prior studies, we take

$$\mathbf{F} = -\kappa_z \frac{dT}{dz} \cdot \mathbf{k}, \quad (16)$$

where z is the vertical coordinate; κ_z is the diffusivity, effectively taken as a function of T since that is the dependence that will allow κ_z to be calculated using [(17)](#); and $\mathbf{k}$ is the vertical unit vector. There are regions in the ocean where surfaces of constant T are nearly vertical, for example in high latitudes. In these regions the fluxes across the surfaces of constant T can be expected to be horizontal rather than vertical. The approach we use here, which has been used in prior estimates, does not account for this effect. As will be seen below, however, the estimate of κ_z obtained assuming [(16)](#) can be interpreted as an upper bound on the vertical diffusivity.

The flux normal to the ocean surface is denoted as $-\mathbf{F} \cdot \mathbf{n} = H$ so that positive H is directed into the ocean. Taking κ_z to be constant in the integration, an estimate for κ_z in the volume V bounded by constant T surfaces T_1 and T_2 is found by substitution in [(11)](#):

$$\kappa_z = \frac{\displaystyle\iint_{B_2} (T - T_2)H \, da - \iint_{B_1} (T - T_1)H \, da}{\left\langle \left(\dfrac{dT}{dz} \right)^2 \right\rangle}$$

$$= \frac{DV}{\left\langle \left(\dfrac{dT}{dz} \right)^2 \right\rangle}. \quad (17)$$

The quantity D can be considered to be more fundamental than κ_z since no assumption concerning the parameterization of $\mathbf{F}$ is involved in determining D.

If the diffusive flux is taken to be three-dimensional and downgradient with positive diffusivity in each direction,

$$\mathbf{F} = -\kappa_x \frac{dT}{dx} \mathbf{i} - \kappa_y \frac{dT}{dy} \mathbf{j} - \kappa_z \frac{dT}{dz} \mathbf{k}, \quad (18)$$

then [(17)](#) gives an estimate for the upper bound of the vertical diffusivity. The estimate made for three-dimensional

diffusion using (11) and (18) is

$$\kappa_z = \frac{DV}{\left\langle \left(\frac{dT}{dz}\right)^2\right\rangle} + \left[\frac{-\kappa_x\left\langle \left(\frac{dT}{dx}\right)^2\right\rangle - \kappa_y\left\langle \left(\frac{dT}{dy}\right)^2\right\rangle}{\left\langle \left(\frac{dT}{dz}\right)^2\right\rangle}\right]. \quad (17a)$$

The additional contribution to the vertical diffusivity from inclusion of the horizontal diffusion [shown in the square brackets in Eq. (17a)] is negative since the horizontal diffusivities are both positive, and the estimate from (17) is larger than the value that would be obtained if the horizontal diffusive fluxes were included.

The estimate (17) provides only a bulk average value of the vertical diffusivity. There is no information on its distribution within a layer. It is likely that larger diffusivities are appropriate for some parts of the layer, such as close to the surface or near topographic features, and smaller diffusivities for other parts, but these considerations are beyond the scope of this study.

Equations (15) and (17) are used to diagnose D and κ_z for temperature and salinity in the ocean. Compressibility effects are neglected in taking temperature to be a conservative tracer. Annual mean tracer fields and surface fluxes are used, ignoring the correlation between the transient components of F and T in the surface integrals of (15) and (17).

The computational procedure, which determines the values of D and κ_z between T_1 and T_2 and the volumes to which these values apply, begins by determining an "outer" volume, the volume enclosed by the surfaces $T = T_2$ and B_2 shown schematically in Fig. 1b ⊙⯐. An outer volume is defined to be composed of volume elements with $T > T_2$ that are touching each other along sides, edges, or corners. There can be more that one physically distinct outer volume found, with the number depending on the structure of T and the value of T_2. The outer surface B_2 is given by those areas where the outer volume reaches the surface of the ocean. Then an "inner" volume is defined to be all volume elements in the outer volume that have $T > T_1$, and the inner surface B_1 is taken as those points of the inner volume that occur at the ocean surface. The volume integrals for the determination of V in (15) and the denominator of the rhs of (17) are carried out over the volume elements that are in the outer volume, but not the inner volume (crosshatched area in Fig. 1b ⊙⯐). The surface integrals are carried out over the outer and inner surfaces. The computations are performed for each physically distinct outer volume that is identified. The above procedure is appropriate only for $T_1 > T_2$, with outer volumes surrounding surface maxima of T. Consequently, the whole procedure is repeated, but for outer and inner volumes surrounding surface T minima, $T_2 > T_1$.

There is a situation introduced by the finite vertical resolution of the data that is given special treatment. When vertical shears, $|dT/dz|$, are large enough, a vertical column that goes through the outer volume can have no volume elements that are not in the inner volume, and therefore these columns will not contribute to the volume integrals. It is important to represent the contribution of these columns in the volume integral in the denominator of the rhs of (17) because the contribution behaves like $(dT/dz)^2 dz$, which in the continuous case increases as the magnitude of the vertical derivative increases and in the case of a discontinuity becomes infinite. When this unresolved high shear situation is encountered, the thickness Δz of the partial volume element that contributes to the integral is estimated by $\Delta z = |(T_2 - T_1)/(dT/dz)|$, and the contribution to the volume integral is taken to be proportional to $|(dT/dz)(T_2 - T_1)|$.

The dissipation method is closely related to the flux method, based on (8), described by Walin (1982) and Niiler and Stevenson (1982), and also employed by Zhang and Talley (1998). However, because (17) provides an upper bound estimate for the vertical diffusivity, the diffusivity method provides additional information.

For verification purposes, the method was applied to output from a multicentury integration with a low-resolution, non-flux-corrected, coupled atmosphere–ocean GCM. Although the model is drifting away from the observed climate, temperature and salinity diffusivities were found to be larger than, but in some volumes close to, the background diffusivities of 0.1×10^{-4} m^2 s^{-1}.

b. Temperature

1) DIFFUSIVITY ESTIMATE

Dissipation and diffusivity of temperature were calculated using observed ocean temperatures from Levitus (1982) and annual-mean net surface heat fluxes from Oberhuber (1988). Heat fluxes for the Arctic and south of 65°S are not included in this dataset and were set to zero for the computations. Missing data elsewhere in the Southern Hemisphere were filled in by linear interpolation. The global mean heat flux of 3.22 W m^{-2}, found by averaging over the World Ocean between 65°S and 60°N, was removed uniformly over this region since the method assumes zero global mean surface flux. A temperature increment of $|T_2 - T_1| = 1°C$ was used. Results using surfaces of constant potential temperature to define the various volumes were indistinguishable from those using temperature.

The temperature diffusivity is shown in Fig. 2a ◉. There are four physically distinct maximum surface temperature volumes (completely surrounded by cooler water and boundaries): the western Pacific warm pool for $T > 29°C$, the Indian Ocean for $T > 28°C$, the eastern Pacific for $T > 28°C$, and the tropical Atlantic for $T > 28°C$. Points with the same symbol will be referred to as "branches." Starting from the high temperature end and proceeding toward lower temperatures along the western Pacific branch, deeper and more extensive volumes of the ocean are involved. The Indian and western Pacific branches merge via the Indonesian throughflow for T between 27° and 28°C. The eastern Pacific warm pool branch merges with the rest of the Pacific between 26° and 27°C. Along the curve that starts in the tropical Atlantic, the volumes grow to encompass the whole deep Atlantic basin as temperature decreases. The Atlantic and Pacific volumes merge into a single near-global volume between 19° and 20°C. The surface heat flux data used in the diffusivity calculation involves physically distinct surface regions for temperatures greater than those where the branches merge. Therefore, errors in the forcing data for the separate temperature maximum branches do not affect the diffusivity estimates in the other branches except at lower temperatures after the branches merge.

There are three physically distinct minimum surface temperature volumes (completely surrounded by warmer water and boundaries), all originating from surface waters between −2° and −1°C. These are found in the Southern Ocean, Weddell Sea, and Arctic Ocean. Diffusivities are not shown for the Arctic and Weddell Sea branches since the Oberhuber climatology does not give data for those regions. However, due to the geometry of the computational procedure, errors in the surface flux data in the surface temperature maximum branches do not affect the results in the surface minimum branches and vice versa. Then, two volumes may be in close physical contact, but independent in the sense of the heat flux data used in the diffusivity calculation. The deep ocean between 1° and 2°C and the Antarctic water between 0° and 1°C are independent in this sense.

The diffusivities along the surface maximum branches generally decrease with decreasing temperature and are less than 0.1×10^{-4} m^2 s^{-1} for $T < 20°C$ in the western Pacific branch. Atlantic and Pacific values are very similar in similar temperature ranges except for smaller diffusivities in the warmest Atlantic water. This correspondence, using forcing and structure data from nonoverlapping surface areas and volumes, could indicate that these values are physically meaningful. On the other hand, negative values are found for the deep water ($1°C < T < 4°C$), which could be an indication of errors in the forcing data. The diffusivities for the warm pool maxima, at the far right of each surface maximum branch, represent geographically localized areas and associated volumes close to the surface. These values exhibit wide variation, with the largest value of more than 4×10^{-4} m^2 s^{-1} in the western Pacific warm pool, an intermediate value in the Indian Ocean, and values near 0.3×10^{-4} m^2 s^{-1} in the eastern Pacific warm pool and tropical Atlantic. This large variation could be due to actual differences in the physical process that control the mixing or could represent errors in the forcing data.

The dissipation from (15) is shown in Fig. 3 ◉. The dissipation tends to be largest in the 24°–26°C volumes and to decrease for both warmer and cooler temperatures. The peak in dissipation for the 24°–26°C temperature range is possibly associated with the large positive contribution from the heat fluxes in the eastern equatorial Atlantic and Pacific. One would expect the dissipation to increase with temperature since the surface to volume ratio decreases with increasing temperature, producing a stronger local mechanical forcing from the atmospheric winds per unit volume as temperature increases. The decrease in dissipation for temperatures in the 26°–30°C range may be due to weaker surface mechanical forcing, as expressed by the smaller friction velocity $[(\tau/\rho)^{1/2}$, not shown], over the warmest ocean waters than over water near 25°C. The mean temperature dissipation for the entire volume of the ocean, obtained from (10) with the integral taken globally and divided by total volume, is 3.3×10^{-9} °C^2 s^{-1}. The volume associated with each of the diffusivities is also shown in Fig. 3 ◉ for reference. The eastern Pacific volumes are small compared to the others, with fluxes over only a small local surface contributing to the dissipation integral. This small size makes the eastern Pacific results less certain.

2) ERROR ESTIMATE

An error estimate was made by calculating the diffusivity with the adjusted net heat flux from da Silva et al. (1995). This second diffusivity estimate is shown in Fig. 2b ◉. The heat flux climatology is defined at all ocean surface points in this data. The global mean of −2.0 W m^{-2} was removed. Above 10°C, both forcing datasets give similar results, with the values

obtained from the da Silva heat flux about 80%–90% of the values found with the Oberhuber heat flux. In contrast to results shown in Fig. 2a ⊙, the diffusivities from the da Silva forcing are positive at all temperatures on the western Pacific branch and become relatively large (0.2×10^{-4} m^2 s^{-1} between 2° and 3°C; 0.56×10^{-4} m^2 s^{-1} between 1° and 2°C) for the deep waters on this branch. The diffusivities for the Southern Ocean and Weddell Sea volumes, however, turn out to be negative using the da Silva heat flux, and those found in the Arctic, while positive, are large (2–7×10^{-4} m^2 s^{-1}).

The procedure of removing the global mean uniformly from the heat flux data is obviously very crude. It is likely that errors are large in some regions and small in others. As pointed out above, the diffusivities from volumes on different branches are independent of the forcing data on other branches. Changing the forcing data in one of these independent volumes does not affect the values found for the diffusivities in the other volumes. For example, changing the heat flux in the Arctic region will not affect the diffusivities along the western Pacific or tropical Atlantic branches. If the global mean is not removed from the forcing data, the resulting diffusivities will be more realistic for the regions with smaller heat flux errors and more unrealistic for the regions with larger errors. Then, calculating the diffusivities using the heat flux data without removing the global mean gives another estimate of the sensitivity of the results to errors in the heat flux data.

Using the Oberhuber heat flux without removing the global mean gives diffusivities 10%–20% larger at warm temperatures than for the Oberhuber heat flux with the global mean removed. Minimum values on the western Pacific branch are 0.14×10^{-4} m^2 s^{-1} in the 16°–20°C classes when the global mean is not removed, about a factor of 2 increase in this temperature range. The diffusivities are most sensitive for water colder then 4°C along the western Pacific branch, with large values found when the global mean in not removed (1.0, 1.9, and 3.9×10^{-4} m^2 s^{-1} for the 3°–4°, 2°–3°, and 1°–2° temperature ranges, respectively). On the other hand, the western Pacific branch diffusivities calculated using the da Silva heat flux without removing the global mean are slightly reduced at the warmest temperatures relative to those found with the global mean removed and are reduced proportionately more at cooler temperatures, becoming small but negative for $T < 14$°C and $<-1 \times 10^{-4}$ m^2 s^{-1} for $T < 3$°C. The Antarctic, Weddell, and Arctic branches (latter two not shown) are not sensitive to the removal of the global mean with the da Silva heat flux.

It is important to note, however, that the sum of the component heat fluxes of da Silva et al. (1995) gives an approximately 30 W m^{-2} global-mean net heat flux into the ocean that is removed uniformly for dynamical consistency in their net heat flux estimate. This large global mean value is presumably in error and is due to much larger regional errors. The effect of the correction by da Silva et al. (1995) is to reduce the diffusivities by about a factor of 2 for $T > 25$°C and to produce increasingly larger reductions for the colder waters.

The greatest sensitivity to errors in the heat flux data is found for the deep water between 1° and 4°C. We cannot determine with any confidence whether the value of the diffusivity appropriate for this region is closer to 0 or to 1×10^{-4} m^2 s^{-1}. Other results, including small diffusivity between 5° and 25°C seem less sensitive. The values for the warmest waters are the least sensitive, but the adjustments made by da Silva et al. (1995) to the heat flux in these regions for dynamical consistency are larger than the sum of the component fluxes, and as noted above the uncertainty in the diffusivities in these regions is at least a factor of 2.

3) COMPARISON WITH RESULTS FROM OTHER INVESTIGATIONS

The Indian Ocean $T > 28$°C value of 1.3–1.5 ($\times 10^{-4}$ m^{-2} s^{-1}), depending on the forcing dataset and whether or not the global mean is removed, is somewhat smaller than the value of 2.2 m^{-2} s^{-1} found by Zhang and Talley (1998) for the diathermal diffusivity of the 28°C surface in the Indian Ocean using the da Silva et al. (1995) heat flux and the flux method. Although the diapycnal diffusivity calculated by Zhang and Talley (1998) involves different volumes of the ocean than the diathermal diffusivity calculated here, the values for roughly comparable volumes seem to be smaller here (e.g., values a factor of 2–3 smaller here in the tropical eastern Pacific surface water, the low-latitude Pacific/Indian and the low-latitude Atlantic). Speer (1997) estimated the minimum diapycnal diffusivity for North Atlantic water near 20°C to be larger than 1×10^{-4} m^2 s^{-1}. This is more than eight times the value we obtain as a maximum for the diathermal diffusivity of all water between 20° and 21°C in the Atlantic. The dissipation integral approach, using surface fluxes and a presumed steady-state three-dimensional tracer distribution, seems to produce results closer to the smaller values obtained from direct microstructure measurements in the ocean interior (Ledwell et al. 1993; Toole et al. 1994; Kunze and Sanford 1996) than from the flux method.

The diffusivity shown in Fig. 2 ⊙ in the upper ocean is similar to that chosen by Bryan and Lewis (1979) for their ocean model. They used a value of 0.3×10^{-4} m^2 s^{-1} in the upper ocean based on tritium estimates of Rooth and Östlund (1972). The range of potential deep ocean values found here is large. The value of 1.3×10^{-4} m^2 s^{-1} chosen by Bryan and Lewis (1979) based on the estimates of Munk (1966) lies within this range.

c. Salinity

Salinity dissipation and diffusivity are evaluated using observed ocean salinity (Levitus 1982) and salinity fluxes (proportional to evaporation minus precipitation, or $E - P$), constructed from latent heat fluxes and precipitation rates from the NCEP (National Centers for Environmental Prediction) reanalysis (Kalnay et al. 1996) climatology. The NCEP reanalysis was used for this calculation because the data produced from direct observations provide insufficient coverage over the Southern Hemisphere oceans to apply the formulas globally. The surface forcing does not include runoff.

The salinity diffusivity results are shown in Fig. 4a, and the associated volumes are shown in Fig. 4b. The diffusivities were calculated for salinity intervals of 1 ppt. The global mean salinity flux corresponding to a net excess of evaporation over precipitation of 0.4 mm day^{-1} was removed uniformly. In contrast to the temperature diffusivity calculations, the salinity diffusivity results were not sensitive to this procedure. The number of separate branches is larger than the number of branches in Fig. 2 because there are more disconnected surface maxima and minima for salinity than was the case for temperature. Values for very small volumes are not shown in Fig. 4.

As in the temperature diffusivity calculations, the volumes are divided into two classes: those associated with surface salinity maxima and those associated with surface minima. The surface maximum branches begin at the far right of the Fig. 4a with salty regions in the South Atlantic, North Atlantic, Arabian Sea, South Pacific, and North Pacific. These branches are all related to each other, combining as indicated, and eventually all merge into a single volume that makes up the bulk of the deep World Ocean (North Atlantic branch at 34–35 psu). Only the North Atlantic branch diffusivities are affected by errors in the forcing for the other branches.

All of the other volumes are associated with surface salinity minima (i.e., points at the left end of the branches). Interconnections between the low salinity branches are not strong. With the exception of the Antarctic and western Pacific/Indonesia branches, the low-salinity branches begin in regions of large river runoff that are not correctly represented in the forcing data. However, errors in the forcing for the low salinity branches do not affect the results in the high salinity branches. In particular, the neglect of river runoff leads to errors in the salinity flux forcing only in the low salinity branches, due to the association of low surface salinity and high river runoff, and does not affect the results in the high salinity branches. It may have been more realistic to distribute the global mean salinity flux imbalance over the surface areas of the minimum volumes rather than uniformly over the whole ocean surface.

The diffusivities along the surface maximum branches shown in Fig. 4 range from 0.4 to 1.7 ($\times 10^{-4}$ m^{-2} s^{-1}). Magnitudes appear to be larger than those for temperature diffusivity in roughly corresponding volumes. The diffusivity for the deep ocean with salinity 34–35 psu is 0.78×10^{-4} m^2 s^{-1} when the global mean forcing is removed and 1.1×10^{-4} m^2 s^{-1} when the global mean forcing is not removed, both of which are close to Munk's (1966) value for the deep ocean. This result depends primarily on precipitation and evaporation generated from 6-h simulations made with an atmospheric GCM initialized with observations of pressure, temperature, humidity, and wind. Spinup of the hydrological cycle is known to be a severe problems in this type of simulation; therefore, there is significant uncertainty in the details of the forcing for the salinity diffusivities. This uncertainty is mitigated, however, by the lack of sensitivity of the diffusivity estimate and the independence of the deep ocean estimate from errors due to the neglect of runoff. Also, the precipitation and evaporation fields appear to be reasonably realistic when compared to independent climatologies or to proxy data such as the observed climatological cloud distribution. As a result, the estimate of the deep ocean salinity diffusivity is probably much less uncertain than the estimate of the deep ocean temperature diffusivity. A conservative estimate of the range in which the actual value of the salinity diffusivity probably falls in the deep ocean volume is then between 0.4×10^{-4} and 1.6×10^{-4} m^2 s^{-1}.

Diffusivities along the surface salinity minimum branches are small, especially in those volumes where runoff should be important. Inclusion of runoff would raise these values, but we have not made quantitative estimates of this effect.

Parameterizations of vertical diffusion of salt and heat for ocean GCMs, such as those included in the GFDL MOM model (Pacanowski 1996), use the same depth-dependent vertical diffusivity for both temperature and salinity. It has been shown by de Szoeke (1998) that equality of the turbulent diffusivities of temperature and salinity would follow from the assumption of the principle of non-negative dissipation of composite tracer variances, as applied to density. Given the uncertainties in the forcing data and the sensitivity of the temperature diffusivity estimates for the deep ocean to errors in the heat flux forcing, our estimates are not inconsistent with taking the same diffusivity for both tracers.

4. Results concerning extrema and homogenization

Some results are developed concerning extrema in and homogenization of the distribution of a tracer T, assuming a steady state and downgradient turbulent diffusion. The Prandtl–Batchelor Theorem is a special case of the first of these results.

First consider the situation when there are no internal source or sinks of T.

1) Homogenization: If there is a volume V bounded by a surface of constant $T = T_1$ and insulating solid boundaries, then $T \equiv T_1$ everywhere inside V.

It follows directly from (10), or equivalently (14) with $f(T) = T^2/2$ and $S = 0$, that, if there is a volume V completely enclosed by a surface of constant $T = T_1$, then

$$\langle \mathbf{F} \cdot \nabla T \rangle = 0. \quad (19)$$

The diffusive flux is assumed to be uniformly down gradient with respect to T so that (18) holds with the κ positive functions of position. Then

$$\mathbf{F} \cdot \nabla T = -\kappa_x \left(\frac{dT}{dx}\right)^2 - \kappa_y \left(\frac{dT}{dy}\right)^2 - \kappa_z \left(\frac{dT}{dz}\right)^2 \le 0 \quad (20)$$

in V. But (19) can only be satisfied if $\nabla T = 0$ everywhere in V. Then T is a constant in V and therefore equal to T_1. If V is bounded by a surface of $T = T_1$ and insulating solid boundaries, then (19) still follows from (10) because $\mathbf{F} = 0$ at the boundary, and homogenization follows as before.

The Prandtl–Batchelor theorem is a special case of this result. Consider a two-dimensional flow with closed streamlines. If diffusion is sufficiently weak, $T = T_1$ along a streamline. Then T is homogeneous in the region bounded by the streamline, proving the Prandtl–Batchelor theorem. The reason that the Prandtl–Batchelor theorem requires weak diffusion can be seen as follows. There is no advective flux across a streamline, so (7) applies inside a closed streamline C, and consequently there is no net diffusive flux across C. However, if diffusion is non-negligible, T need not be constant on C, and (10) does not hold. The major formal difference between the Prandtl–Batchelor theorem and the configuration considered here is that the Prandtl–Batchelor theorem is applied to closed streamlines as opposed to constant T surfaces. In practice, the Prandtl–Batchelor theorem is a prognostic relationship since any bounded steady two-dimensional flow has closed streamlines. On the other hand, the results developed here are diagnostic since it is not necessary a priori that the T distribution contains the structure considered.

If there is a region enclosed by a surface of constant $T = T_1$ and T is observed to vary in this region, then it may be inferred either that the flow is not in a steady state, that there are sources/sinks of T in the region, or that the diffusive flux is not monotonic in the gradient of T.

2) Extrema: There can be no extrema of T in the interior or at an insulating solid boundary.

If there is an extremum in the interior, then this extremum can be enclosed by a surface of constant $T = T_1$. However, then T is homogeneous inside T_1, as proven above, which contradicts the assertion that there is an extremum. If the extremum is assumed to occur at an insulating solid boundary, then it can be enclosed by a surface of constant $T = T_1$ and the boundary, also contradicting the homogenization result.

3) Existence of sources: If there is an extremum of T in the interior, there must be a collocated source S, $S > 0$ for a maximum or $S < 0$ for a minimum. If there is a volume V of homogeneous T then $S \equiv 0$ in V.

With the steady state and downgradient conditions satisfied, the assumption of nonzero S must be violated for an extremum to exist. If there is an interior extremum, it can be enclosed by a surface of constant $T = T_1$. Then it follows from (14) with $f = T^2/2$, (13), and (20) that $\langle (T - T_1)S \rangle > 0$. The T_1 surface may be taken to enclose an arbitrarily small volume containing the extremum. Then a maximum $(T > T_1)$ can only occur where there is a source, $S > 0$, and a minimum, $T < T_1$, can only occur where there is a sink, $S < 0$. A region of homogenous T must have S identically zero, and T cannot be homogenous where S is nonzero, since both advective and diffusive flux divergences vanish locally in a region of homogenous T, leaving nothing to balance S in (1).

4) Extrema at a boundary: If there is an extremum of T on the boundary, there must be a collocated outward normal boundary flux F, $F < 0$ for a maximum or $F > 0$ for a minimum. If there is a volume V of homogeneous T adjacent to a

boundary then $F \equiv 0$ where V meets that boundary.

With the steady state and downgradient conditions satisfied, the assumption of nonzero F must be violated for an extremum to exist at the boundary. The extremum, can be enclosed by a surface of constant $T = T_1$. Then it follows from [(10)](#) and [(20)](#) that $\iint_B (T - T_1)(\mathbf{F} \cdot \mathbf{n})\, da < 0$. The T_1 surface may be taken to enclose an arbitrarily small volume containing the extremum. Then a maximum $(T > T_1)$ can only occur where the flux is inward, $\mathbf{F} \cdot \mathbf{n} < 0$, and a minimum $(T < T_1)$ can only occur where the flux is outward $\mathbf{F} \cdot \mathbf{n} > 0$. A region of homogenous T must have $\mathbf{F} \cdot \mathbf{n}$ identically zero if it is adjacent to the boundary, since diffusive fluxes vanish locally in a region of homogenous T, and normal advective fluxes are zero at the boundary, leaving nothing to locally balance a nonzero flux across the boundary.

5)   The maximum and minimum values of T found in the interior also are found on the noninsulating boundary. All values of T found in the interior occur on the noninsulating boundary if that boundary forms a single connected surface.

Suppose a homogenous volume with $T = T_1$ is found in the interior and that this volume is "isolated" (i.e., has an extreme value) in the sense that $T < T_1$ in the surrounding volume. Then, as in 2) the homogeneous volume can be enclosed by a surface of constant T_2 with $T_2 < T_1$ everywhere on the surface. But then T is homogeneous everywhere inside the enclosing volume with $T = T_2 \neq T_1$, which is a contradiction. The analogous argument applies to a homogeneous volume surrounded by a volume $T > T_1$, as well as when the homogeneous volume is adjacent to insulating boundaries. Then the homogeneous volume cannot be isolated in the interior or adjacent to insulating boundaries, and $T = T_1$ somewhere on *any* enclosing surface. Taking the enclosing surface to be the physical boundaries of the fluid, the result that both the lowest and the highest interior values must occur at a boundary follows. This boundary must be noninsulating by the result of 4). If the noninsulating boundary forms a single connected surface, then all values of T found in the interior also occur on this surface by continuity.

If there are multiple disconnected noninsulating boundaries, then there can be nonextreme values of T found in the interior that do not occur on a noninsulating boundary. A simple example of this case is steady one-dimensional diffusion with different values of T specified at top and bottom boundaries.

5. A weak inference about ocean structure

Due to the long timescale for adjustment of the deep ocean (thousands of years) and the much shorter period of intensive observation of the deep ocean (tens of years), there is no guarantee that the deep ocean climatology obtained from the observations is in a steady state rather than a "rapidly" changing (relative to the ocean's adjustment time) transient state. However, it is usually assumed in climate modeling and in interpretation of paleoclimate data that today's ocean is in an equilibrium steady state. Consequently, the deep oceans of coupled climate models are typically spun up for tens of thousands of simulated years in order to approach an equilibrium (e.g., [Manabe et al. 1990](#); [Bryan 1998](#)). The results developed in [section 4](#) can be applied to tracers in the ocean to determine whether their climatological distributions are broadly consistent with a steady state and downgradient turbulent diffusion. The appropriate averaging time for the climatology would be several decades, which is long compared to the internal dynamical timescales, such as those of waves and eddies, but short compared to the ocean adjustment time.

The climatological salinity from [Levitus (1982)](#) was searched for extrema. Since sources and sinks of salinity are thought to be negligible below the surface, then, if a subsurface extremum or isolated homogeneous volume is found or if the extreme values found in the interior are not found at the boundary, one of the assumptions of the extremum results of [section 4](#), either steady-state or downgradient diffusion, must be violated. Similarly, if boundary extrema are not locally anticorrelated with outward boundary fluxes, then one of those assumptions must be violated. If interior extrema are not found and boundary extrema are appropriately correlated with boundary fluxes, then this is evidence that the ocean is consistent with a steady state and turbulent salinity transfer down the mean salinity gradient. The test was not carried out for temperature, since the dynamical constraint of gravitational stability will prevent the occurrence of interior density extrema even in a transient circulation, and density and temperature variations are closely related. Of course, salinity has a significant role in the density stratification, so salinity is not an ideal tracer for this test either.

Below the surface, the only pronounced salinity extremum is a maximum at about 770 m in the Atlantic along the coast of Spain, which is known to be due to the Mediterranean outflow (the Mediterranean is not connected to the Atlantic in our interpolation of the data). Other than that, only very weak extrema were found below the surface in regions that were close to connecting to surface values. At the surface, there are several pronounced maxima in the subtropics of each hemisphere, which all coincide with positive surface salinity flux in the reanalysis $E - P$ data. There are also surface minima located in regions of negative $E - P$, including the tropical rain belt and the high latitudes of both hemispheres. Many surface minima

are located near the coasts, where they are also associated with river outflow. Then there are no prominent interior extrema, and the maxima or minima at the boundaries are associated with positive or negative boundary salinity fluxes, respectively. We conclude that the climatological salinity distribution of the oceans is consistent with being in a steady-state balance between advection by the time mean flow and downgradient turbulent diffusion, with sources and sinks at the upper boundary and a deep boundary source in the Mediterranean outflow.

These extremum tests are necessary conditions for the structure to be in a steady state. They are, however, not sufficient. In other words, it is possible to generate cases with downgradient diffusion in which there are no internal extrema, and the boundary flux/tracer distribution correlation is negative, but in which the tracer distribution is not in a steady state. For example, any state is valid for the tracer and surface flux distributions as an initial condition for an ocean GCM, and the general initial condition that satisfies the extremum test will be transient.

6. Summary

A relationship between volume integrated dissipation rate and the covariance between the turbulent tracer fluxes and tracer distribution along the boundaries was derived for volumes bounded by surfaces of constant tracer concentration. Assuming that the turbulent fluxes are represented by downgradient k theory gives an estimate of the upper bound for bulk vertical diffusivities in these volumes. The method does not provide any information on the distribution of the diffusivity within the volumes or on the processes responsible for the dissipation. The dissipation rates are more fundamental than the diffusivities in that they do not depend on assumptions about the spatial distribution of the diffusion coefficients.

Dissipation and diffusivity were estimated for temperature in the ocean, using the three-dimensional climatological temperature distribution and the net surface heat flux as input data. The dissipation per unit volume was found to be maximum between 24° and 26°C in both the Atlantic and Pacific/Indian Oceans. The diffusivity was found to be $O(0.1 \times 10^{-4} \text{ m}^{-2} \text{ s}^{-1})$ for temperatures between 5° and 20°C, with larger values at warmer temperatures. In a test using two different heat flux analyses, the diffusivity above 5°C did not show large sensitivity to potential errors in the forcing data. However, the diffusivities at all temperatures were sensitive to adjustments of the magnitude required to remove the global mean (30 W m^{-2}) from one of the heat flux datasets. Similar values of diffusivity were diagnosed for the Atlantic and Pacific/Indian Oceans between 19° and 27°C using independent data. This coincidence lends some confidence to these estimates. At colder temperatures, which include the bulk of the deep ocean, the estimated diffusivity was highly sensitive to small changes in the forcing data.

Estimates were also made for upper bounds for salinity diffusivity as a function of salinity. Evaporation minus precipitation from an atmospheric reanalysis was used for salinity flux forcing since areal coverage of observed data is insufficient. The contribution from runoff was not adequately addressed in these estimates. The salinity diffusivity for the deep ocean was found to be $O(1.0 \times 10^{-4} \text{ m}^{-2} \text{ s}^{-1})$. However, this estimate was not affected by the runoff problem and also appeared not to be highly sensitive to errors in the forcing. Therefore, this estimate is probably reasonably realistic.

Assuming a steady state and downgradient diffusion, some results were developed concerning extrema in and homogenization of the distribution of a tracer T:

1. With no internal sources or sinks, there can be no extrema of T in the interior or at insulating boundaries. If a volume is bounded by a surface of constant T, then T must be homogenous everywhere inside that surface.

2. If there is an interior extremum, then there must be a collocated source of the appropriate sign. Similarly, a boundary extremum must be collocated with a surface flux of the appropriate sign. If there is a homogenous region, there can be no source or sink in that region. A boundary adjacent to a homogenized volume must be insulating.

3. The extreme interior values of T will also be found at the noninsulating boundary, and all interior values of T will be found at the noninsulating boundary if this forms a single connected surface.

The Prandtl–Batchelor theorem can be obtained from (1) for two dimensions and in the limit of small diffusivity.
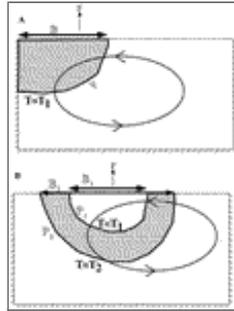
The annual average salinity distribution of Levitus (1982) was examined for extrema. No significant (given the problems of spatial and temporal sampling) extrema were found in the interior. A subsurface maximum was found in the Atlantic near Spain associated with the Mediterranean outflow (in the interpolated salinity data the Mediterranean is not connected to the rest of the World Ocean). Also several extrema were found at the surface, with maxima or minima associated with surface salinity fluxes into or out of the ocean, respectively. The salinity distribution is then consistent with the assumptions a steady-state ocean in which turbulent transfer is downgradient with respect to the time mean salinity. However, it is also possible to construct transient salinity distributions that have no internal extrema, with downgradient turbulent transfer and no internal sources, so the lack of internal extrema is not sufficient to infer a steady state.


REFERENCES

Batchelor, G. K., 1956: On steady laminar flow with closed streamlines at large Reynolds numbers. *J. Fluid Mech.,* **1,** 177–190..

Bryan, F. O., 1998: Climate drift in a multicentury integration of the NCAR Climate System Model. *J. Climate,* **11,** 1455–1471.. Find this article online

Bryan, K., and L. J. Lewis, 1979: A water mass model of the world ocean. *J. Geophys. Res.,* **84,** 2503–2517..

da Silva, A. M., C. C. Young, and S. Levitus, 1995: *Atlas of Surface Marine Data 1994.* Vol. 1: *Algorithms and Procedures,* NOAA Atlas NESDIS 6, 83 pp..

de Szoeke, R. A., 1998: The dissipation of fluctuating tracer variances. *J. Phys. Oceanogr.,* **28,** 2064–2074.. Find this article online

Garrett, C., K. Speer, and E. Tragou, 1995: The relationship between water mass formation and the surface buoyancy flux, with application to Phillips' Red Sea model. *J. Phys. Oceanogr.,* **25,** 1696–1705.. Find this article online

Hide, R., 1969: Dynamics of the atmospheres of the major planets with an appendix on the viscous boundary layer at the rigid bounding surface of an electrically-conducting rotating fluid in the presence of a magnetic field. *J. Atmos. Sci.,* **26,** 841–853.. Find this article online

Joyce, T. M., 1980: On production and dissipation of thermal variance in the oceans. *J. Phys. Oceanogr.,* **10,** 460–463.. Find this article online

Kalnay, E., and Coauthors, 1996: The NCEP/NCAR 40-Year Reanalysis Project. *Bull. Amer. Meteor. Soc.,* **77,** 437–471.. Find this article online

Kunze, E., and T. B. Sanford, 1996: Abyssal mixing: Where it is not. *J. Phys. Oceanogr.,* **26,** 2286–2296.. Find this article online

Ledwell, J. R., A. J. Watson, and C. S. Law, 1993: Evidence for slow mixing across the pycnocline from an open-ocean tracer-release experiment. *Nature,* **364,** 701–703..

Levitus, S., 1982: *Climatological Atlas of the World Ocean.* NOAA Prof. Paper No. 13. U.S. Dept. of Commerce, 173 pp..

Manabe, S., K. Bryan, and M. J. Spelman, 1990: Transient response of a global ocean–atmosphere model to a doubling of atmospheric carbon dioxide. *J. Phys. Oceanogr.,* **20,** 722–749.. Find this article online

Munk, W. H., 1966: Abyssal recipes. *Deep-Sea Res.,* **13,** 707–730..

Niiler, P., and J. Stevenson, 1982: The heat budget of tropical ocean warm-water pools. *J. Mar. Res.,* **40** (Suppl.), 465–480..

Oberhuber, J. M., 1988: An atlas based on the 'COADS' data set: The budgets of heat, buoyancy and turbulent kinetic energy at the surface of the global ocean. Max-Planck-Institut für Meteorologie, Hamburg, Rep. 15, 199 pp..

Pacanowski, R. C., 1996: MOM 2 version 2.0 (beta) documentation user's guide and reference manual. GFDL Ocean Tech. Rep. 3.2. [Available from GFDL/NOAA, Princeton University, Princeton, NJ 08542]..

Pedlosky, J., 1996: *Ocean Circulation Theory.* Springer Verlag, 453 pp..

Rooth, C. G., and H. G. Östlund, 1972: Penetration of tritium into the Atlantic thermocline. *Deep-Sea Res.,* **19,** 481–492..

Schneider, E. K., 1977: Axially symmetric steady state models of the basic state for instability and climate studies. Part II: Nonlinear calculations. *J. Atmos. Sci.,* **34,** 280–292.. Find this article online

Speer, K. G., 1997: A note on average cross-isopycnal mixing in the North Atlantic ocean. *Deep-Sea Res.,* **44,** 1981–1990..

Stern, M. E., 1975: *Ocean Circulation Physics.* Academic, 246 pp..

Toole, J. M., K. L. Polzin, and R. W. Schmitt, 1994: Estimates of diapycnal mixing in the abyssal ocean. *Science,* **264,** 1120–1123..

Walin, G., 1982: On the relation between sea-surface heat flow and thermal circulation in the ocean. *Tellus,* **34,** 187–195..

Zhang, H.-M., and L. D. Talley, 1998: Heat and buoyancy budgets and mixing rates in the upper thermocline of the Indian and global oceans. *J. Phys. Oceanogr.,* **28,** 1961–1978.. Find this article online

Figures

Click on thumbnail for full-sized image.

Fig. 1. Schematic views of the regions discussed in the text. The steady flow is represented by the elliptical contours with arrows. The physical boundaries of the fluid are given by the bounding rectangles, with insulating boundaries surrounded by diagonal cross-hatching. The volume integrated over in Eq. (4) is shown by the horizontally cross-hatched region in (a), enclosed by the indicated parts of the solid boundary B and the surface P of constant $T = T_1$. The surface flux F out of that region across noninsulating solid boundaries is also indicated. The horizontally cross-hatched region in (b) represents the volume integrated over in Eq. (11). The surfaces B_1 and B_2 indicate the areas over which the surface flux contributions are calculated.
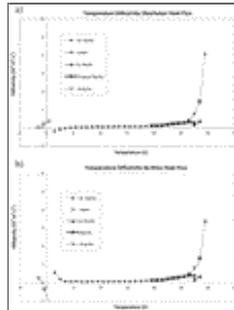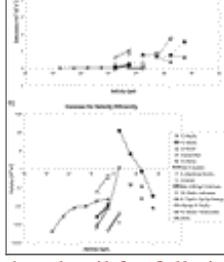

Click on thumbnail for full-sized image.

Fig. 2. Vertical temperature diffusivity κ_z as a function of temperature found from (17) for 1°C intervals using Levitus (1982) temperature. The net surface heat flux is from (a) Oberhuber (1988) and (b) da Silva et al. (1995). The branches are labeled according to the location of extreme SST values, maxima for western Pacific, Indian, eastern Pacific, and tropical Atlantic Oceans, and minimum for the Southern Oceans. The lines connecting the data points represent some of the data dependencies of the layers with respect to the diffusivity calculation.
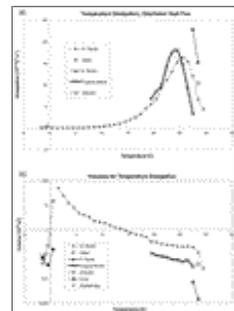
Click on thumbnail for full-sized image.

Fig. 3. (a) Plot of D as a function of temperature as defined by (15) for the same volumes and surface flux as in Fig. 2 and (b) volumes as a function of temperature corresponding to the results in Figs. 2 and 3a. The Arctic and Weddell Sea volumes, for which there is no surface forcing data, are also shown.

Fig. 4. (a) Vertical salinity diffusivity as a function of salinity found from (17) for 1-ppt intervals using NCEP reanalysis climatological precipitation minus evaporation and Levitus (1982) salinity. (b) Volume as a function of salinity corresponding to the results in Fig. 4a ⊙⋅. The points and curves are labeled according to the location of surface extreme values.

Corresponding author address: Edwin K. Schneider, Center for Ocean–Land–Atmosphere Studies, 4041 Powder Mill Rd., Suite 302, Calverton, MD 20705-3106.

E-mail: schneide@cola.iges.org